Design and Implementation of a Laparoscope Calibration Method for Augmented Reality Navigation

M. Schwalbe[1], *M. Fusaglia*[1], *P. Tinguely*[2], *H. Lu*[1], *S. Weber*[1]

[1] *ARTORG Center for Biomedical Engineering, University of Bern, Switzerland*
[2] *Department of Visceral Surgery, University Hospital of Bern, Switzerland*

Kontakt: marius.schwalbe@artorg.unibe.ch

Abstract:

Intraoperative laparoscopic calibration remains a challenging task. In this work we present a new method and instrumentation for intraoperative camera calibration. Contrary to conventional calibration methods, the proposed technique allows intraoperative laparoscope calibration from single perspective observations, resulting in a standardized scheme for calibrating in a clinical scenario. Results show an average displacement error of 0.52 ± 0.19 *mm, indicating sufficient accuracy for clinical use. Additionally, the proposed method is validated clinically by performing a calibration during the surgery.*

Keywords: laparoscope calibration, augmented reality, navigation system

1 Problem

Augmented reality (AR) and image-guided surgery (IGS) in laparoscopic procedures merges preoperative 3D organ reconstructions with the intraoperative laparoscopic video, in a single, coherent view. To obtain a real-time AR view, the preoperative 3D reconstruction has to be rendered at the same perspective of a laparoscope. Therefore the laparoscope is tracked by the IGS system and the camera needs to be calibrated. Camera calibration attempts to find the extrinsic and intrinsic parameters (i.e. 3D pose of the camera and optical properties respectively), which results in recovering the image pose and therefore enable AR to be accomplished.

The camera calibration problem has been well studied for general computer vision applications. Tsai [1] presented a two-stage calibration technique that efficiently solve the intrinsic and extrinsic parameters. It is achieved by establishing a real constraint to reduce the dimensionality of the unknown parameter space. Zhang [2] proposed an alternative approach where camera calibration is achieved by observing a tracked planar object of known dimensions through the laparoscope from different perspectives. These observations yield in a set of 2D points which are used to solve a formulation of the camera parameters.

These calibration techniques have also been applied for laparoscope calibration [3, 4, 5, 6]. However, the main challenge of bringing the technique into clinics is the simplicity of use and the sufficient accuracy for surgical safety. Additionally, the sterile barrier between the surgical instruments and these calibration objects also hinder the integration of such techniques in the surgical scenario.

We believe that to increase the acceptance of AR techniques in the operating room (OR), a standardized calibration technique which allows a reproducible and accurate laparoscope calibration in the clinical settings has to be developed. The goal of the calibration is to entirely know the 3D pose of the laparoscopic image in the OR. Therefore the transformation of the camera optics to the marker (i.e. extrinsics) and the optical properties of the laparoscope (i.e. intrinsics) need to be determined once.

Within this work we present a new calibration method and instrumentation that allows intraoperative laparoscope calibration from single perspective observation. Additionally, we evaluate the accuracy and reproducibility of the calibration results together with its integration in the operating scenario.

2 Material and Methods

2.1 Device Design and Conceptual Workflow

An existing navigation system (CAS-One, CAScination AG, Bern, Switzerland) dedicated for liver surgery [7] with an infrared-based optical tracking (Polaris Vicra, Northern Digital, Waterloo, Ontario, Canada) was used. The laparoscope (OTV-S7P, Olympus, Shinjuku, Tokio, Japan) was tracked via a marker shield with four retro-reflective spheres attached onto the rigid scope.

A laparoscope calibration unit (LCU) composed of a peek planar dotted pattern attached to a titanium body containing a channel and retro-reflective spheres was developed (the LCU can be seen on the left in

Figure 1). The peek pattern is composed of a laser engraved grid of 8 × 12 dots (dot size of 3 mm) which is automatically detected in the laparoscopic image. The channel on the titanium body allows the easy placement of the laparoscope to obtain images of the grid from different distances.

The design of the calibration unit and the graphical user interface (GUI) facilitates the laparoscope calibration workflow in the surgical scenario without the help of a technician. By positioning the laparoscope within the proximity of the LCU, the GUI is automatically triggered by the tracking system. The surgeon is then guided through the entire process without any touch-screen interactions. To acquire the four images at predefined distances, guidance information are given in the form of arrows, textual commands and sound notifications to control the positioning of the laparoscope in the LCU channel (the acquired images can be seen in Figure 2 top).

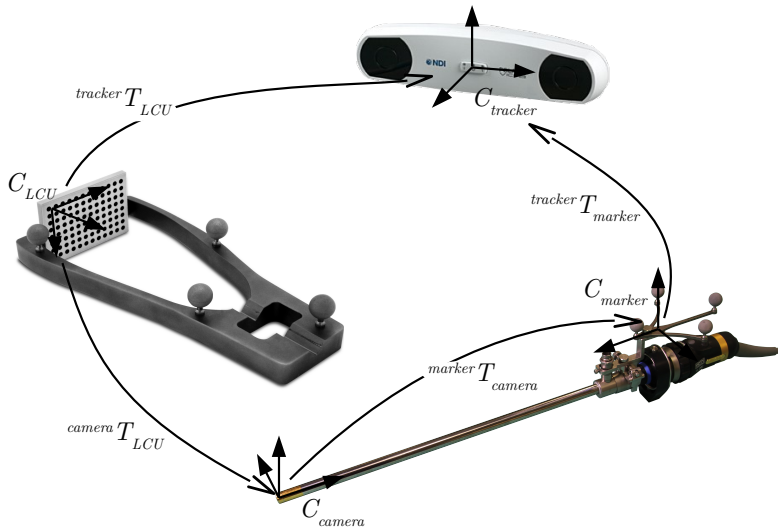

Figure 1: Diagram describing the transformations involved in the laparoscope calibration process.

2.2 Algorithmic Solution

To achieve a single perspective calibration, we propose a preprocessing algorithmic step to generate artificial independent planes, representing the calibration grid (i.e. their transformations are not related by pure translation). These planes, obtained through the tracking knowledge, are thereafter used to perform the camera calibration method in [2] to get an initial guess.

For this approach the images are handled as a set of points instead of individual images. Since the transformations from the tracking can be recorded in addition (see Figure 1), they can be used to compute a 3D position for each of the points in a unique coordinate system.

Therefore, the 3D points can be transformed from the LCU grid coordinate system C_{LCU} to the laparoscope marker coordinates C_{marker} by applying the transformation ${}^{tracker}T^{-1}_{marker} . {}^{tracker}T_{LCU}$. This results in a point cloud which forms roughly[1] the volume of a cuboid (see Figure 2 bottom).

The camera calibration then computes the intrinsic and extrinsic parameters. The extrinsic matrix maps the 3D points from the coordinate system C_{LCU} to the camera coordinates C_{camera} (i.e. ${}^{camera}T_{LCU}$ is the extrinsic matrix).

Since we have transformed the points into the coordinate system of the laparoscope marker C_{marker}, the extrinsic matrix is the transformation from the laparoscope coordinate system C_{marker} to the camera coordinate system C_{camera}:

$$ {}^{marker}T^{-1}_{camera} = {}^{camera}T_{LCU} . {}^{tracker}T^{-1}_{LCU} . {}^{tracker}T_{marker} $$

Note that it is essential, that the artificial point sets are planar, in order to find the transformations from the planes in the 3D space to the points of the planes in the images, because they are transformed using homographies.

[1] since the rotation of the laparoscope around its image axis is not completely restricted, the individual point grids can be slightly rotated

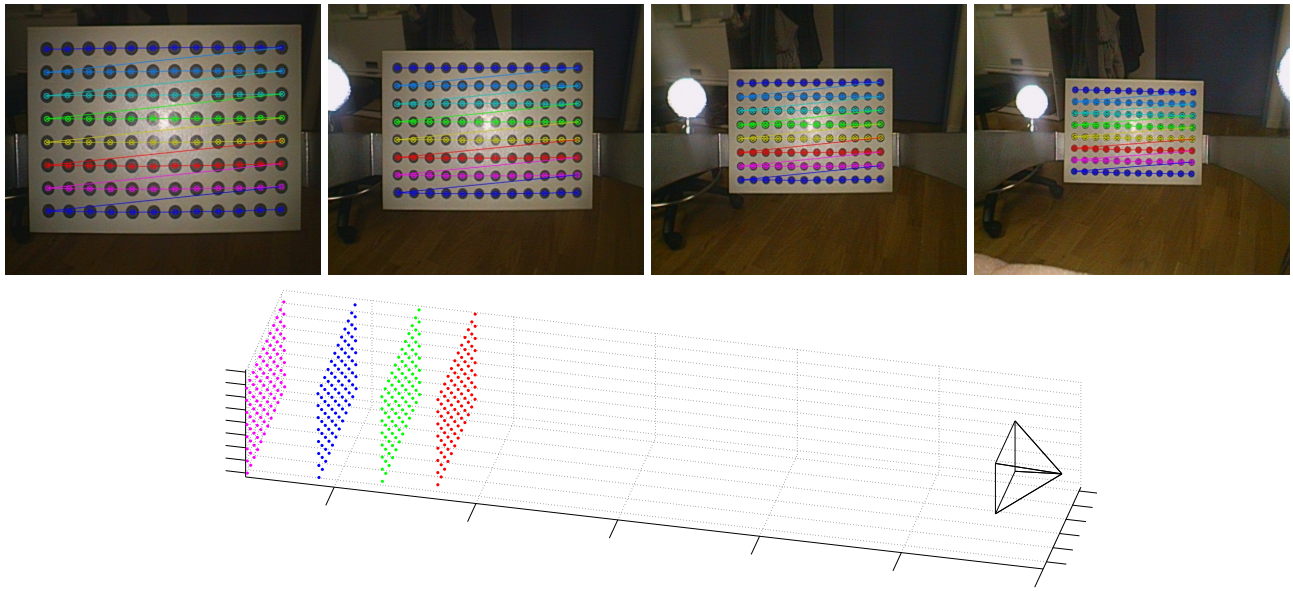

Figure 2: Top: the original images acquired for the calibration with the detected dots. Bottom: the setup: on the right is the camera frame of the laparoscope and on the left the positions of the point grid at four different distances. All points together form the cuboid like point cloud.

Each of the acquired point sets $P^{(k)}$, $k \in \{1, \ldots, n\}$ from the $n = 4$ images are planar, but their transformations are related by pure translations (to denote a matrix or vector belonging to a specific image k of the original images $\{1, \ldots, n\}$ superscript indices in brackets $^{(k)}$ will be used).

Since all points are projected into the common coordinate system of the laparoscope, all of them will be used as one point set $\mathscr{P} = \bigcup_k P^{(k)}$.

Starting from the point set $\mathscr{P}$, artificial planes which have independent transformations are created. For each of the artificial planes three points $A, B, C \in \mathscr{P}$ are selected from the point cloud. The points A, B, C have to be non-collinear to span a plane. The normal of the plane is given by the normalized vector $\vec{n} = (\vec{b} - \vec{a}) \times (\vec{c} - \vec{a})$, where $\vec{a}, \vec{b}, \vec{c}$ are the position vectors of the points A, B, C.

This is done for every artificial plane $l \in \{1, \ldots, p\}$, where p is the number of artificial planes to be used (similar to the $^{(k)}$ for the matrices or vectors belonging to a specific image k of the original images $\{1, \ldots, n\}$ superscript indices in brackets $^{(l)}$ will be used to refer to an artificial plane l).

The plane l can be described by the equation $\left(\vec{x} - \vec{a}^{(l)}\right) \cdot \vec{n}^{(l)} = 0$, where $\vec{a}^{(l)}$ is the position vector of one of the points, $\vec{n}^{(l)}$ the normal for plane l and $\vec{x}$ any point that lies on this plane. We create artificial planes out of the four remaining sides of the cuboid like point cloud and the four diagonals which are visible from the camera. An illustration of these $p = 8$ planes can be seen in Figure 3.

Since in the first step of the calibration a homography has to be computed for every plane, at least four points are needed on each of the artificial planes. Therefore for every artificial plane $l \in \{1, \ldots, p\}$ the subset of points from the point cloud $\mathscr{P}$, that lie closer than a certain threshold ϵ to the plane, is computed:

$$P^{(l)} = \left\{ x \in \mathscr{P} \;\middle|\; \left(\vec{x} - \vec{a}^{(l)}\right) \cdot \vec{n}^{(l)} < \epsilon \right\}.$$

For every point $M \in \mathscr{P}$ the corresponding image point m is known. That implies that for every set $P^{(l)}$ of 3D points the set $p^{(l)}$ of the corresponding image points is available.

In summary this gives new planar point sets $P^{(l)}$ in 3D and their corresponding point sets $p^{(l)}$ in the image domain. Using this, a camera calibration method [2] can be performed. Using the intrinsic and extrinsic parameters as initial guess, the Levenberg-Marquardt optimization algorithm [8, 9] is applied using all points (the set $\mathscr{P}$ and the corresponding points in the image domain), because not all of them are included in one of the planes $P^{(l)}$, $l \in \{1, \ldots, p\}$.

The entire algorithm was implemented using the OpenCV library [10] and integrated into the CAS-One navigation system.

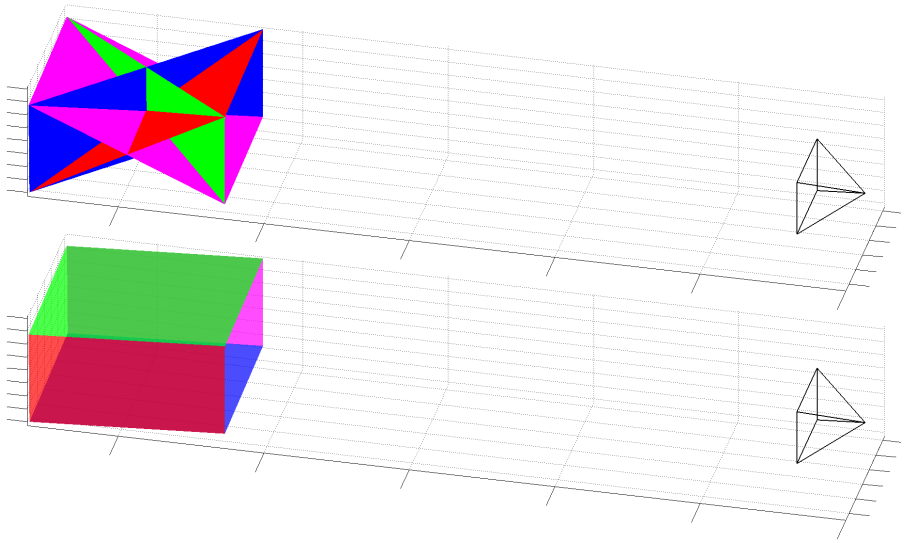

Figure 3: The artificial planes used. There are two types of planes: on the top the diagonal planes and at the bottom the outer planes from the point cloud.

2.3 Experiments

Accuracy and reproducibility of the calibration were evaluated by performing 10 calibration attempts in a controlled environment. For each attempt 4 images were acquired at distances of 60, 85, 110 and 135 mm from the tip of the laparoscope to the plane.

Within the calibration attempts, the laparoscope was fixed with a clamp to maintain the same position during the whole experiment. All the poses of the LCU for the calibration and the evaluation were predefined and controlled using a numerical control machine.

The evaluation of each calibration attempt was performed by acquiring a second set of 12 images of the circle grid in different poses including translations and rotations. For all the 12 images the dots were detected and an overlay computed. From these two information the displacement error in millimeters was derived.

Clinical applicability and workflow of the laparoscope calibration was evaluated during one navigated laparoscopic liver ablation by measuring the time to perform the laparoscope calibration and number of attempts to obtain an accurate calibration.

3 Results

3.1 Accuracy and Reproducibility

All ten calibrations were successful, i.e. in none of the cases the calibration had to be restarted or failed. The average displacement error over all 12 evaluation images was 0.52 ± 0.19 mm.

From the distribution of the average displacement errors for the individual poses over all ten calibrations (see Figure 4) it can be seen that the errors significantly varies depending on the pose of the LCU.

For a pure translation ($P1$ to $P4$) the median error is small (all below 0.24 mm). For small rotations of the LCU ($< 15°$, $P5$ and $P6$) it differs depending on the distance (0.2 mm vs. 0.47 mm) but is still small (having a maximum of 0.73 mm for one calibration). For the larger rotations of the LCU ($> 30°$, $P7$ to $P10$) the median error is always below 0.87 mm. Just for the poses 11 and 12 the errors are frequently larger than 1 mm. We assume that this is due to a disadvantageous pose of the LCU for the tracking, e.g. at the border of the tracking volume (for more information about the accuracy variation of optical tracking the reader is referred to [11]):.

Moreover all ten calibrations perform equally for the different poses (the maximal IQR[2] is 0.28 mm; again at pose 12). Furthermore by investigating the distributions of the intrinsic and extrinsic camera parameters over all the calibrations, it is possible to notice that they are quite stable.

With the exception of the principal point (u_0, v_0) all of them have a small IQR (focal lengths ≤ 1.07 px, extrinsic translations ≤ 0.26 mm and extrinsic rotations $\leq 0.61°$). The IQR of the principal point is as expected

[2]interquartile range, the range in which the middle 50% of the values are located; in the boxplot this is exactly the height of the box

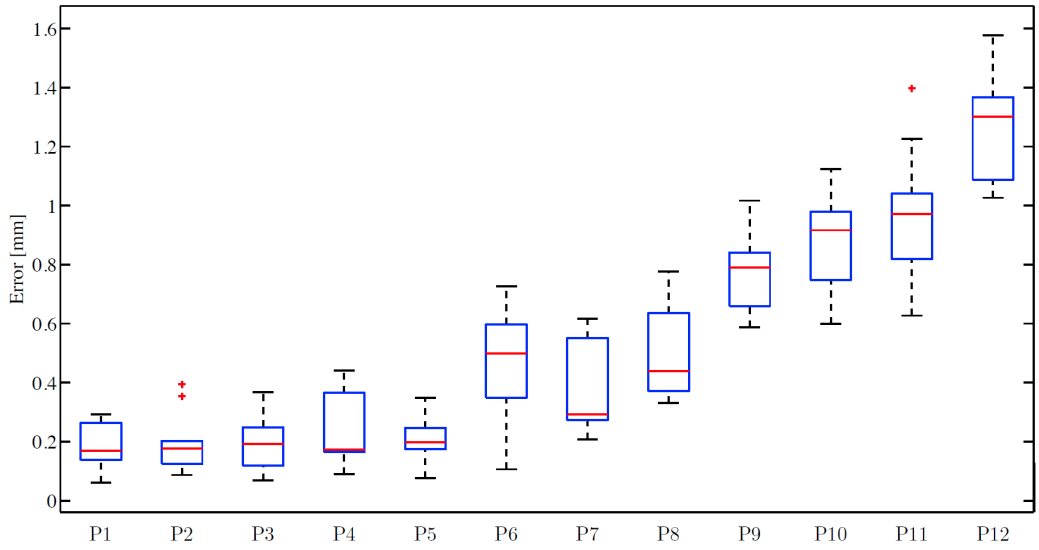

Figure 4: The distributions of the errors per pose. All of them have a small IQR (the height of the boxes is relatively small) and the medians differs a lot depending on the pose.

larger, especially on the u axes of the image (4.36 px). The principal point is the intersection of the optical axis of the camera with the image plane. The pose of the laparoscope is measured at the camera head and includes also the direction of the optical axis.

By assuming that the optical tracking system has an accuracy of 0.2 mm, and since the marker for the laparoscope has a diameter of 85 mm, it is possible to derive an angular accuracy of $\tan^{-1}(0.2/85) = 0.135°$. The distance from the marker to the plane of the LCU during the calibration is on average 450 mm. This implies that the tracking error for the positions of the principal point during calibration is $450 \cdot \tan(0.135) = 450 \cdot 0.2/85 = 1.06$ mm, which is approximately five times larger than for all other parameters involved in the calibration. This corresponds with the results, e.g. 0.94 px IQR for the focal length f_u and 4.36 px IQR in the u direction for the principal point.

3.2 Clinical Evaluation

The LCU did not report any damage from sterilization via autoclave, proving the effectiveness of the design. The time required for mounting the LCU was within 1 minute (see Figure 5). Intraoperatively five laparoscope calibration attempts were performed within 38 seconds on average (14 – 63 sec). In one of the five attempts the calibration failed.

Figure 5: Left: camera calibration in the operating room with a sterilizable prototype of the LCU. The LCU is placed directly on the belly of the patient allowing the laparoscope to be positioned at its natural operating pose. Right: displaying the overlay of the liver in the OR after the successful calibration.

4 Discussion

In this work, we propose a laparoscope calibration method and unit, which can be used intra-operatively by the surgeon. Contrary to state of the art method [2], only a translation of the calibration plane is needed for the proposed method.

The rotation of the plane is simulated by using information from the optical tracking of the laparoscope calibration unit (LCU) and the laparoscope to derive artificial planes. These artificial planes are related by transformations, including rotations. They are then used to perform a full calibration, giving the intrinsic and extrinsic parameters of the laparoscope.

In order to acquire a set of four images of the calibration plane at different distances, a sterilizable prototype of the LCU was developed. It consists of a fixed plane with a dot grid on it, a chamfer to guide the laparoscope during the camera calibration and retro-reflective spheres for the optical tracking.

Through experiments it was verified that the laparoscope calibration is accurate and reproducible. The average displacement error is 0.52 mm (with a maximum of 0.67 mm) and the average IQR is 0.19 mm (with a maximum of 0.28 mm). In addition the method is reproducible over different calibration procedures.

From the experiments we find that the tracking has a huge influence on the calibration. Due to the laparoscope's size the tracking error is at the tip of the laparoscope approximately five times larger than at the marker. This results in a large variance for the principal point.

Moreover, the displacement error of the overlay is highly influenced by the pose of the laparoscope in the view volume of the optical tracking. Especially by tilting the laparoscope after calibration, the displacement error increases.

The feasibility of performing a calibration in sterile conditions was proven by performing fast (avg. 38 sec) and accurate calibrations intraoperatively at the University Hospital of Bern.

5 References

[1] R. Y. Tsai, "A versatile camera calibration technique for high-accuracy 3d machine vision metrology using off-the-shelf tv cameras and lenses," *IEEE Journal of Robotics and Automation*, vol. 3, no. 4, pp. 323–344, 1987.

[2] Z. Zhang, "Flexible camera calibration by viewing a plane from unknown orientations," in *International Conference on Computer Vision (ICCV'99)*, vol. 1, pp. 666–673, 1999.

[3] S. De Buck, J. Van Cleynenbreugel, I. Geys, T. Koninckx, P. Koninck, and P. Suetens, "A system to support laparoscopic surgery by augmented reality visualization," in *MICCAI 2001*, vol. 2208, pp. 691–698, Springer Berlin Heidelberg, 2001.

[4] R. Shahidi, M. Bax, J. Maurer, C.R., J. Johnson, E. Wilkinson, B. Wang, J. West, M. Citardi, K. Manwaring, and R. Khadem, "Implementation, calibration and accuracy testing of an image-enhanced endoscopy system," *Medical Imaging, IEEE Transactions on*, vol. 21, no. 12, pp. 1524–1535, 2002.

[5] C. Wengert, M. Reeff, P. Cattin, and G. Szkely, "Fully automatic endoscope calibration for intraoperative use," in *Bildverarbeitung fr die Medizin 2006*, pp. 419–423, Springer Berlin Heidelberg, 2006.

[6] R. Melo, J. Barreto, and G. Falcao, "A new solution for camera calibration and real-time image distortion correction in medical endoscopy: Initial technical evaluation," *Biomedical Engineering, IEEE Transactions on*, vol. 59, pp. 634–644, March 2012.

[7] M. Peterhans, A. vom Berg, B. Dagon, D. Inderbitzin, C. Baur, D. Candinas, and S. Weber, "A navigation system for open liver surgery: design, workflow and first clinical applications," *The International Journal of Medical Robotics and Computer Assisted Surgery*, vol. 7, no. 1, pp. 7–16, 2011.

[8] K. Levenberg, "A method for the solution of certain non-linear problems in least squares," *Quarterly Journal of Applied Mathmatics*, vol. II, no. 2, pp. 164–168, 1944.

[9] D. W. Marquardt, "An algorithm for least-squares estimation of nonlinear parameters," *SIAM Journal on Applied Mathematics*, vol. 11, no. 2, pp. 431–441, 1963.

[10] "OpenCV: Camera Calibration and 3D Reconstruction," August 2013.

[11] A. D. Wiles, D. G. Thompson, and D. D. Frantz, "Accuracy assessment and interpretation for optical tracking systems," 2004.